A Grid-based Simulation Model for the Evolution of Influenza A Viruses

Hsin-Ting Chung[1] and Yuh-Jyh Hu[1,2]
[1]*Institute of Biomedical Engineering, National Chiao Tung University, 1001 University Rd., Hsinchu, Taiwan*
[2]*College of Computer Science, National Chiao Tung University, 1001 University Rd., Hsinchu, Taiwan*

Keywords: Influenza A Viruses, Evolution, Mutation, Simulation.

Abstract: We propose a simulation approach for analyzing and predicting the evolution of influenza A viruses (IAVs). The simulation is conducted in a sequence-based space to constrain the evolutionary trends within a grid of clusters of protein sequences. The simulated trajectories enable the investigation into point mutations on a protein strain of IAVs in evolution, which cannot be accomplished easily by analyses of phylogenetic trees. We tested the simulation model on three IAV internal proteins, NP, PB1 and PB2. The produced evolutionary pathways were consistent with previous studies of the reassortment history of the 2009 human pandemic. In addition, the chronological analysis of host-associated signature mutations on NP, PB1 and PB2 also agreed with the previous findings.

1 INTRODUCTION

Influenza viruses belong to the viral family Orthomyxoviridae, which includes seven genera: influenza A, influenza B, influenza C, influenza D, Thogotovirus, Isavirus and Quaranjavirus. The accumulation of point mutations during genome replication, and the reassortment of viral gene segments during mixed infections, promote the evolution of influenza viruses (Naffakh *et al.*, 2008).

Influenza A viruses (IAVs) have the capacity to evade host immune systems because of a wide variety of potential combinations of the 18 HA and 11 NA subtypes. Precursors to future pandemics could be viruses carrying the HA subtypes H1, H2, H3, H5, H6, H7, H9, H10, and NA subtypes N1, N2, N3, N8 that have been known to cause outbreaks or sporadic human infections. Because of their vast genetic diversity and unique host range, IAV have caused recurrent annual epidemics and several major worldwide pandemics in human history. The emergence and spread of novel IAV remain of major global concern; therefore, increased understanding of the evolutionary trajectories is essential to maintain the efficacy of antiviral drugs and influenza vaccines (Timofeeva et al., 2017).

Most phenotypic evolution within species as well as most morphological, physiological, and behavioural differences between species can be explained by adaptation due to natural selection (Gerrish, 2001). To respond to a change in environments, the task of adaption for a species is to move the population from its current state toward the new phenotypical optimum state.

Phylogenetic trees have been widely used to show the evolutionary relationships between different or distant species with a common anscestor. Successful applications of phylogenetic trees to the study of IAV evolution include identification of epistatic interactions (Neverov et al., 2015) and development of predictive fitness models for HA (Łuksza & Lässig, 2014). Unlike previous works, this paper presents a new approach for analyzing IAV evolution by addressing the evolutionary dynamics of IAV in terms of the gradual accumulation of point mutations in sequences toward the new phenotypical optimum state.

2 MATERIALS AND METHODS

We model the simulation of IAV evolution in a sequence-based space (Gillespie, 1984; Orr, 2002), and constrain the simulated evolutionary trends in a grid of clusters of protein sequences. Figure 1 shows a sample simulated evolutionary trajectory on a grid for a viral protein. The Y-axis indicates the specific host species, and the X-axis represents the timescale.

Chung, H. and Hu, Y.
A Grid-based Simulation Model for the Evolution of Influenza A Viruses.
DOI: 10.5220/0008878401090116
In *Proceedings of the 13th International Joint Conference on Biomedical Engineering Systems and Technologies (BIOSTEC 2020) - Volume 3: BIOINFORMATICS*, pages 109-116
ISBN: 978-989-758-398-8; ISSN: 2184-4305

This evolutionary trajectory in Figure 1 shows that the wild type protein started first as a segment in an avian virus strain. It then went through the reassortment events caused by cross-species mutations, and finally evolved into a segment in the 2009 S-OIV human pandemic virus.

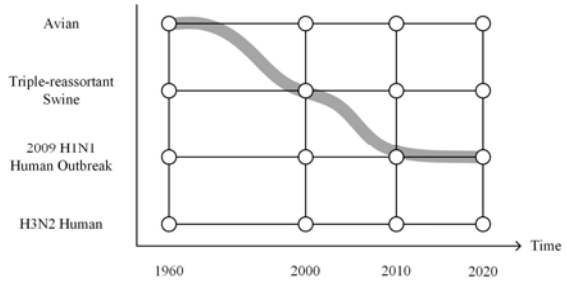

Figure 1: A sample evolutionary trajectory.

2.1 Construction of Evolutionary Grids

A simulated evolutionary trajectory is produced by a stochastic process that is controlled within the grid. A node in a grid, as shown in Figure 1, represents a cluster of proteins that have high similarities according to some metric, such as sequence similarity, temporal, or geographical distributions, etc. Different designs of evolutionary grids, such as the number of nodes, the members in a node, and the time interval between nodes, exert different influences over the stochastic simulation process, which warrants its flexibility.

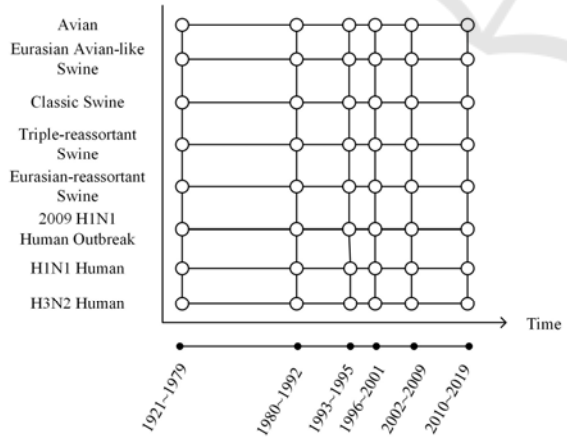

Figure 2: A sample design of an evolutionary grid.

To construct an evolutionary grid, we first determine the types of viruses to study and the intervals on the time line to set up the framework of a grid. Figure 2 shows a grid designed for the study of viruses of various host species, e.g. classic swine. The time line is divided into six intervals, e.g. 1921~1979. After the framework of a grid is determined, to complete the construction is to create the protein clusters for the nodes on the grid. These clusters together with the grid framework control the stochastic simulation.

We first constructed a phylogenetic tree for the IAV sequences downloaded from NCBI and GISAID EpiFlu. Based on the phylogenetic analyses (Smith et al., 2009) of human, swine and avian sample sets, we assigned these sampled sequences (287 human, 115 swine and 411 avian) as the seeds to the appropriate clusters according to their isolation years and subtypes. For example, A PB1 protein 36_H1N1_Swine_swine_ohio_23_1935 in this case was assigned to the node located at X-coordinate= "1921~1979" and Y-coordinate= "classic swine" as shown in Figure 2. Based on the locations of these seeds in the phylogenic tree, we identified from the phylogenic tree the lowest common ancestor (LCA) per host species and subtype. For each LCA in ascending order of its distance to the root, we iteratively assigned the remaining sequences under the LCA to the corresponding cluster on the grid. The coordinate on the Y-axis was determined by the LCA's host species or subtype, and the isolation year determined the coordinate on the X-axis. We illustrate the process of host species assignment in Figure 3 with an example of 10 seed sequences and 7 others. We start with Avian LCA, which is the closest to the root. All sequences under the LCA except the seeds are assigned to Avian, including the left-most sequence in the tree. We next assign the remaining sequences under Human LCA to H3N2 Human. Finally, we process those non-seed sequences under Swine LCA. Note the left-most sequence in the tree is then reassigned to Swine from Avian. The final host species assignments are presented at the bottom of the tree, as shown in Figure 3, and their coordinates on the timescale X-axis are determined by the isolation years. We postprocess the clusters by removing sequences with amino acid similarity exceeding a certain threshold (set to 0.99) using CD-HIT (Li & Godzik, 2006).

2.2 Grid-based Stochastic Simulation

We conduct a stochastic process in the sequence-based space to simulate a point mutation that is constrained by an evolutionary grid. By performing a series of stochastic processes to simulate the accumulation of point mutations, we can generate a simulated evolutionary trajectory for a wild type IAV protein.

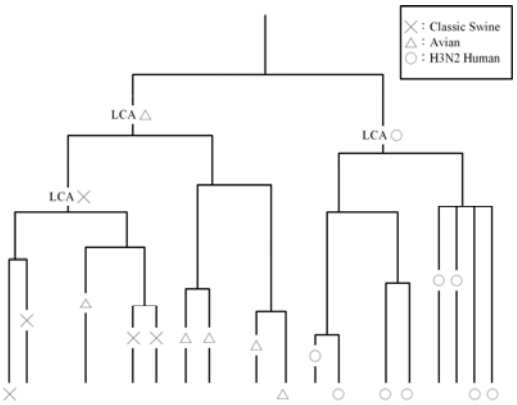

Figure 3: A sample process of host species assignment. The seed sequences are denoted by a symbol within the vertical bars, e.g. the 2nd ×(Classic Swine) to the left. The others are the remaining sequences to be assigned to a host species.

2.2.1 Point Mutation and Adaptive Walks

The adaptive walk and mutation landscape models (Gillespie, 1991; Orr, 2003, 2006) assume that a current wild-type sequence represents a local optimum. After an environment change, the fitness of this wild-type sequence drops, and its adaption is required. A wild type IAV sequence of L amino acids has 19L one-point mutants. To complete a beneficial point mutation in adaption, one favorable mutant sequence is stochastically selected based on the fitness, and substituted for the current wild type.

The fitness is assigned to each one-point mutant in two steps. First, for a given wild-type sequence, we form a neighborhood of k nearest neighbors according to sequence similarity. The details of constructing a neighborhood is described in the next section. We compute the average sequence similarity between the k-nearest neighbors and each of the 19L one-point mutants. Second, we generate and sort 19L+1 random fitnesses based on a specified probability distribution (e.g. normal, Gamma or exponential). The i^{th} value is reserved for the current wild type, where i can be set to 10, 50 or 150 as in (Orr, 2002), and the remaining sorted 19L values are assigned to the 19L one-point mutants individually in descending order of sequence similarity computed earlier. The 1st to the (i-1)th one-point mutants in the sorted list are considered the beneficial mutants as they have higher fitness than the current wild type. Figure 4 illustrates the process of fitness assignment.

After the assignment of the fitnesses is complete, we calculate the mutation probability P_t that the current wild type (i.e. the i^{th} sequence) mutates to the t^{th} one-point mutant ($t = 1 \sim i$-1) in the sorted list. We define the probability P_t as follows.

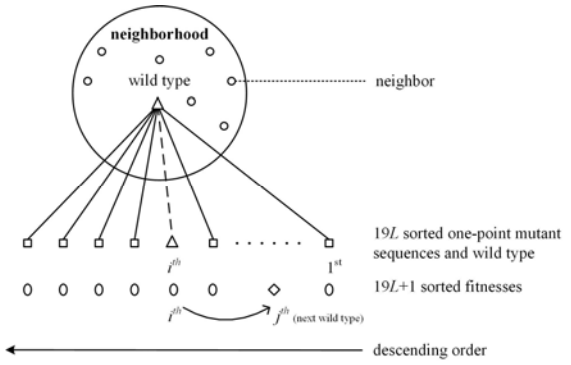

Figure 4: Fitness assignment.

$$P_t = \frac{\Pi_t}{\Pi_1 + \Pi_2 + \Pi_3 + \cdots + \Pi_{i-1}} \quad (1)$$

$$\Pi_v = 1 - exp^{-2S_v} \quad (2)$$

$$S_m = \frac{F_m - F_i}{1 + F_i}, \text{where } m = 1 \ldots i - 1 \quad (3)$$

where F_r is the fitness of the r^{th} one-point mutant sequence, S_m is the selection coefficient of the m^{th} one-point mutant sequence, and Π_v is the probability of fixation for the m^{th} one-point mutant sequence, as defined in Orr (Orr, 2002) and Gillespie (Gillespie, 1983). We select one of the beneficial mutants randomly as the next wild-type sequence based on the probability distribution of P_t to implement a stochastic point mutation. The fitness of the next wild type (i.e. j^{th} mutant as in Fig. 4) becomes the stopping threshold for the next point mutation in an adaptive walk. To check if one-point mutation should continue, we generate a new set of 19L+1 random fitnesses. If the current threshold is higher than all the fitnesses, it indicates a convergence and we stop point mutation; otherwise, we repeat the same point mutation process as above. When a new wild type is fitter than all its one-point mutants, an adaptive walk is complete, and the fixation of the fittest wild-type sequence represents a local optimum. This status remains until the environment changes again. It will then trigger a new adaptive walk, and the evolution continues. All these adaptive walks connected together form a simulated evolutionary trajectory of the initial wild type.

Unlike previous works that focused on mutational landscapes, adaption patterns and fitness distributions (Gillespie, 1991; Orr, 2002; Orr, 2006), our study of adaption considers sequence similarity, which enables us to describe the accumulation of point mutations along a simulated evolutionary trajectory. Figure 5 shows the process of an adaptive walk.

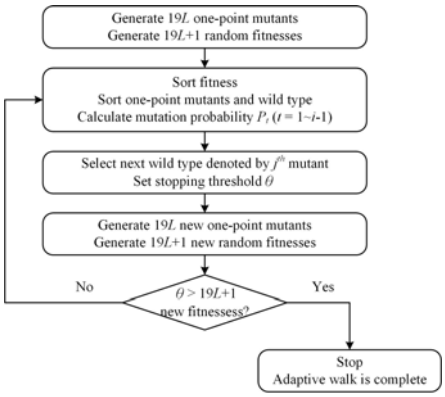

Figure 5: Process of an adaptive walk.

2.2.2 *K*-nearest-neighbor Neighborhood

As mentioned in the previous section, we sort the 19*L* one-point mutants according to their sequence similarities to a neighbourhood of *k*-nearest neighbors. Because the ranking of the mutants is crucial to the result of point mutation, the members in the neighborhood consequently play an important role in the control of adaptive walks.

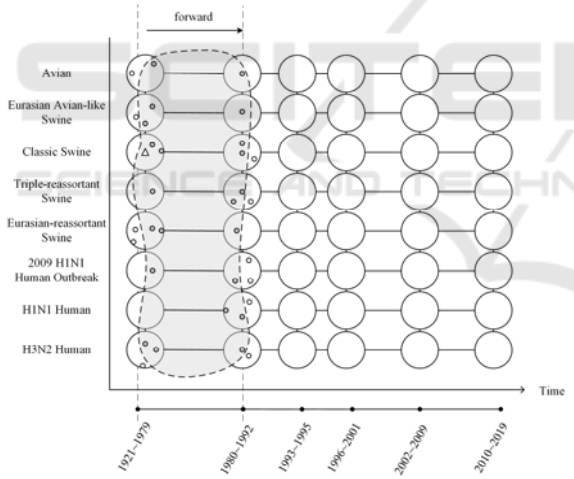

Figure 6: Construction of neighbourhood for retrospective simulation. The triangle denotes the initial wild type isolated in 1978. The shaded area represents a forward *k*-nearest-neighbor neighborhood.

We classify the simulated evolutionary trajectories into two types: retrospective and prospective. A retrospective trajectory describes the events of point mutation that may have occurred to a given wild type. By contrast, a prospective trajectory predicts the events of point mutation that may occur in the near future to some current wild type. The *k*-nearest-neighbor neighborhood is therefore constructed differently for retrospective and prospective simulations.

For retrospective simulation, we construct a neighborhood from the sequences available on the evolutionary grid. Given a wild-type sequence, we first identify its closest mapping sequence on the grid. For this closest sequence, to form a neighborhood we locate its *k*-nearest neighbors on the grid that were isolated in the same year or later to warrant the adaptive walk will move forward in time. We call these neighbors "forward neighbors."

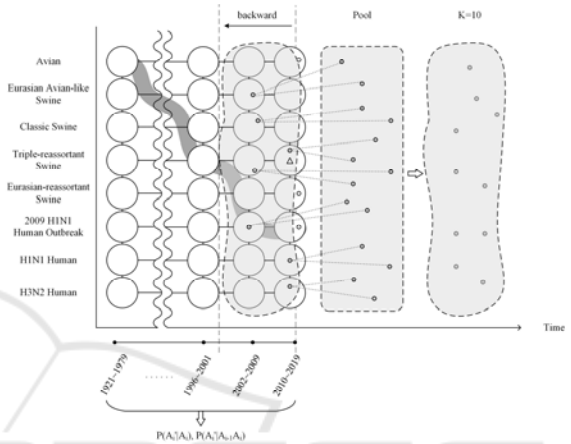

Figure 7: Construction of neighbourhood for prospective simulation. The triangle denotes the wild type of interest isolated in 2010. The irregular shaded area to the left represents a backward *k*-nearest-neighbor neighborhood. The middle rectangular shaded area indicates a pool from which to create a pseudoneighborhood. The irregular shaded area to the right shows a *k*-nearest-neighbor pseudoneighborhood.

Unlike retrospective simulation, it is not appropriate to construct a neighborhood directly from the sequences available on the grid because they were isolated in the past, and they may mislead the adaptive walk backward in time. To resolve the problem with unavailability of forward neighbors, we create pseudoneighbors. For a current wild type of interest, we select a sequence available on the grid as an initial wild type, and run retrospective simulation multiple times until the simulated evolution reaches the given wild type of interest or some similar sequence. If the retrospective evolution cannot reach the given wild type or even a similar sequence, we start with a different initial wild type and repeat the retrospective simulation. We collect the amino acid mutation frequencies from the retrospective trajectories, and estimate the first-order and second-order transition probabilities of amino acids, $P(AA_i' \mid AA_i)$ and $P(AA_i' \mid AA_{i-1}\ AA_i)$, where AA is an old

amino acid, AA' is the new amino acid after point mutation, and *i* is the position of the amino acid in the sequence.

In contrast to the *k*-nearest-neighbor neighborhood identified in retrospective simulation, to create a pseudoneighborhood for a wild type of interest, we first identify its *k*-nearest sequences that are available on the grid and were isolated in the same year or earlier than this wild type. We call these neighbors "backward neighbors." From each backward neighbor sequence, we generate multiple pseudosequences based on the first-order and second-order transition probabilities, and collect them into a pool. Subsequently, we select from the pool the *k*-nearest pseudosequences to the wild type to construct the pseudoneighborhood. Figures 6 and 7 illustrate the construction of neighborhoods for retrospective and prospective simulation, respectively.

3 RESULTS AND DISCUSSION

We tested the proposed simulation model on three internal proteins, PB1, PB2, and NP, of IAVs. For each protein, we selected four different strains and tested them in retrospective and prospective simulations, respectively. Table 1 lists the protein strains in the study.

Table 1: List of protein strains for simulation tests.

Internal Protein (Host)	Strain Name (retrospective simulation)	Strain Name (prospective simulation)
PB1 (Human)	A/nt/60/1968 A/England/878/1969 A/Memphis/101/1972 A/England/1972	A/Waikato/16/2000 A/New South Wales/36/2000 A/Queensland/6/2000 A/Western Australia/12/2000
PB2 (Avian)	A/pintail duck/ALB/219/1977 A/mallard/Alberta/46/1977 A/duck/Alberta/35/1976 A/mallard/Wisconsin/524/1979	A/duck/NJ/7717-70/1995 A/mallard/Minnesota/282/2000 A/common teal/Netherlands/10/2000 A/shorebird/Delaware Bay/280/1999
NP (Swine)	A/swine/Italy/2/1979 A/swine/Wisconsin/1/1967 A/swine/Tennessee/19/1976 A/swine/Illinois/1/1975	A/swine/Wisconsin/125/97 A/swine/Wisconsin/464/98 A/Swine/Iowa/533/99 A/swine/North Carolina/47834/2000

For both retrospective and prospective simulations, we set the isolation year of the strain as the start year, and 2018 as the end year. The simulation model was evaluated from two perspectives on the evolutionary trajectories. One was the interspecies-transition pathway on a timescale; the other was the mutation on IAV genomic signatures. Unlike conventional phylogenetic tree analyses, a simulated evolutionary trajectory of an IAV is able to show when an interspecies transition may have occurred or will occur, and what the mutations on the amino acids are.

3.1 Analysis of Interspecies Transitions

We conducted the analysis differently according to the type of evolutionary trajectories, retrospective or prospective.

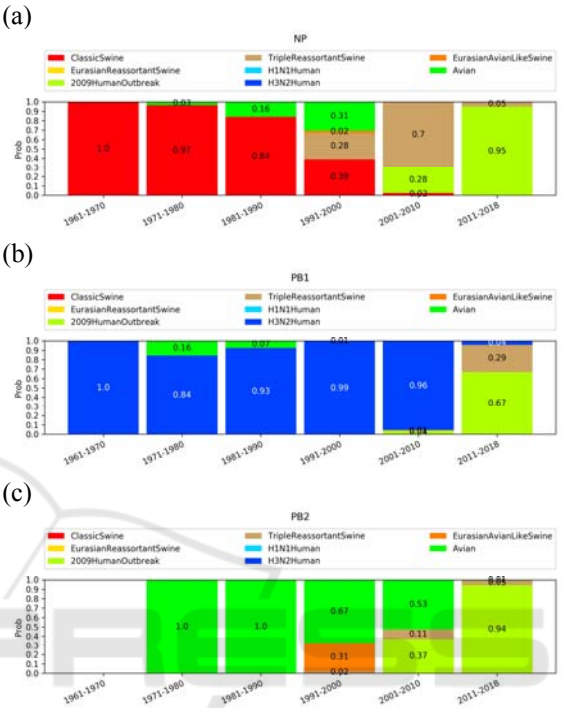

Figure 8: Retrospective evolutionary pathways. (a) NP, (b) PB1 and (c) PB2.

Each retrospective simulation started with the isolation year of the selected protein strain, and was aborted when it reached the year 2018. For each protein strain, we repeated the same simulation 10 times, and visualized the stochastic evolutionary pathways in Figure 8. We divided the timescale into intervals. The height of a rectangular bar in different colors represents the probability of a host species (and subtype) for a protein mutant within an interval. For example, in Figure 8(a) during 2011-2018 the probabilities of the host species, swine (TripleReassortantSwine) and human (2009HumanOutbreak), for an NP protein mutant are 0.05 and 0.95, respectively. We estimated the probabilities from the ten simulated evolutionary pathways. For each NP mutant during 2011-2018 on the 10 evolutionary pathways, we first identified *q* (*q* set to 40 in this study) real NP protein sequences isolated during 2011-2018 from NCBI and GISAID EpiFlu that are most similar to this mutant. We subsequently derived the host species probabilities

for an NP mutant from the proportions of these top-*q* real sequences according to their host species and subtypes.

(a)

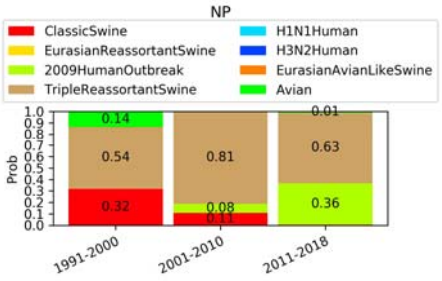

(b)

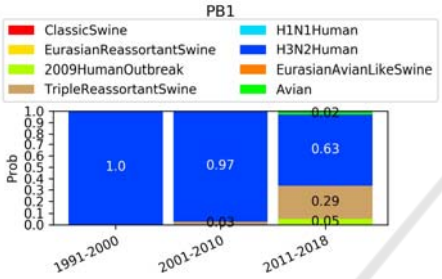

(c)

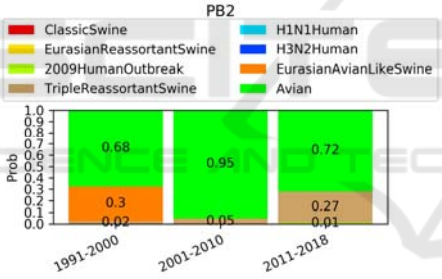

Figure 9: Prospective evolutionary pathways. (a) NP, (b) PB1 and (c) PB2.

We noted a marked rise in the probability of TripleReassortantSwine during 1991-2000 for NP proteins (28%), as shown in Figure 8(a). In addition, the probability of 2009HumanOutbreak increased to 28% during 2001-2010, and reached 95% in the final interval. Our simulation results of interspecies transitions were consistent with the previous study that the reassortment events may have occurred during 1990-2001 and led to the human pandemic in 2009 (Smith *et al.*, 2009). By contrast, Figure 8(b) and (c) show that the probabilities of TripleReassortantSwine during 1991-2000 were infinitesimal for PB1 (< 1%) and PB2 (2%). Not until the final two intervals, 2001-2010 and 2011-2018, did the probabilities of TripleReassortantSwine and 2009HumanOutbreak become noticeable. These discrepancies may be attributable to the genetic variabilities in internal proteins that our simulation failed to address due to the small number of protein strains in our current study.

To evaluate the predictive performance of prospective simulations, we selected protein strains isolated during 1995-2000. For each strain, we first conducted 10 retrospective simulations to estimate the transition probabilities of amino acids from the evolutionary trajectories. For each strain we simulated 10 prospective pathways starting from its isolation year to 2018 based on the estimated transition probabilities. Note that the construction of the prospective pathways for a protein strain did not depend on any other real strains available but isolated later than the strain in test. Therefore, these prospective pathways were considered the predictions about this protein strain, and their validity could be verified by previous studies of IAVs. For example, a simulated prospective pathway of A/Waikato/16/2000 provides a prediction of its potential interspecies transitions after 2000. We summarize the results in Figure 9.

Similar to the results of the retrospective simulations in Figure 8(a), Figure 9(a) shows the highest probability of TripleReassortantSwine for NP proteins during 1991-2000 and 2001-2010 in the prospective simulations. The probability of 2009HumanOutbreak started to increase during 2001-2010, and became more evident during 2011-2018, which was in accordance with the temporal reconstruction of the reassortment history of the 2009 human pandemic (Smith *et al.*, 2009). We also observed from Figure 9(b) that the first reassortment of swine lineages with PB1 proteins occurred during 2001-2010. The predicted interval agreed well with the previous finding that a new triple reassortant swine virus was first detected in 1998 (Brown *et al.*, 1998). In comparison with Figure 8(c), Figure 9(c) shows similar probability distributions of the host species during 1991-2000. While the interspecies transition to 2009HumanOutbreak did not occur until 2011-2018, and the probability was small (1%), as shown in Figure 9(c), the predicted interval was close to when the outbreak occurred.

3.2 Analysis of Mutation on Genomic Signatures

The establishment of an influenza virus in a new host is rare because it requires the efficient and effective transmission, replication, and adaptation of the virus. Nevertheless, pandemics caused by widely circulating viruses with the potential to transmit to humans remain a threat (Naffakh *et al.*, 2008). Unlike

the analysis of molecular mechanisms, using in vitro systems and reverse genetics of influenza viruses, the analysis of a continuously increasing amount of available viral sequence data enables a cost-effective approach for the identification of genomic signatures as host-range determinants (Hu *et al.*, 2014). Genomic signatures can change because of point mutations and interspecies reassortment. The simulation model could provide a deeper insight into the transitions of these signatures, and increase our understanding of the adaption trends.

Table 2: Results of genomic signature mutations based on retrospective evolutionary trajectory analysis. (a) NP, (b) PB1 and (c) PB2.

(a)

NP	Swine ↓ Human	Interval					
position	AA mutation	1961 | 1970	1971 | 1980	1981 | 1990	1991 | 2000	2001 | 2010	2011 | 2018
313	F→V	0	0	0	0	17	70
	F→Y	0	0	0	0	0	1
109	I→V	0	0	0	0	0	100
217	I→V	0	0	0	23	68	219
353	V→I	0	0	0	63	24	10

(b)

PB1	Swine ↓ Human	Interval					
position	AA mutation	1961 | 1970	1971 | 1980	1981 | 1990	1991 | 2000	2001 | 2010	2011 | 2018
327	R→K	1	25	8	108	331	4

(c)

PB2	Avian ↓ Human	Interval					
position	AA mutation	1961 | 1970	1971 | 1980	1981 | 1990	1991 | 2000	2001 | 2010	2011 | 2018
271	T→A	0	0	0	72	61	2
588	A→T	0	0	0	87	74	2
684	A→S	0	0	0	0	29	16
453	P→S	0	0	0	0	32	36
292	I→V	0	2	16	61	55	59
	I→T	0	0	0	0	0	3
475	L→M	0	0	14	54	1	31
559	T→I	0	0	0	0	26	7
590	G→S	0	0	0	0	53	1

We examined the retrospective and prospective evolutionary trajectories for the mutations on the host-associated signatures that have been identified in previous studies (Miotto *et al.*, 2010; Hu *et al.*, 2014; Pan *et al.*, 2009). Seventeen and one amino acid signatures have been identified on NP and PB1 proteins, respectively, to separate swine influenza viruses from human influenza viruses. Twenty amino acid signatures have been found on PB2 proteins to distinguish avian influenza viruses from human influenza viruses.

Table 3: Results of genomic signature mutations based on prospective evolutionary trajectory analysis. (a) NP, (b) PB1 and (c) PB2.

(a)

NP	Swine ↓ Human	Interval		
position	AA mutation	1991 | 2000	2001 | 2010	2011 | 2018
109	I→V	0	10	2
217	I→V	0	3	3
353	V→I	10	29	9
	V→S	0	0	4
344	S→L	0	0	1

(b)

PB1	Swine ↓ Human	Interval		
position	AA mutation	1991 | 2000	2001 | 2010	2011 | 2018
327	R→K	2	76	74

(c)

PB2	Avian ↓ Human	Interval		
position	AA mutation	1991 | 2000	2001 | 2010	2011 | 2018
271	T→A	0	2	9
292	I→V	99	132	48
	I→T	6	10	3
475	L→M	83	72	29
368	R→K	0	1	0
613	V→T	7	24	30
199	A→S	0	1	2
674	A→T	0	0	2
702	K→R	5	50	31
44	A→S	0	1	3
661	A→T	0	2	1

We checked each host-associated signature on NP, PB1 and PB2 along the simulated evolutionary trajectories, retrospective and prospective, respectively. From all the simulated trajectories, we recorded the frequency of signature mutations within each time interval. We identified from the retrospective trajectories 4 NP signatures, 8 PB2 signatures, and the one PB1 signature. In addition, we also identified 4 NP signatures, 10 PB2 signatures, and the same PB1 signature from the prospective trajectories. They all showed at least one mutation at some time on the evolutionary trajectories, and different frequencies of mutations in different intervals. We summarize the results in Tables 2 and 3. For example, Table 2(a) shows that on all the simulated retrospective trajectories of NP, 17 occurrences of amino acid mutation from F to V were identified during 2001-2010.

By comparing Table 2 with Table 3, we observed that most of the signature mutations identified from the prospective trajectories were coincident with those identified from the retrospective trajectories. Three out of four NP signatures found from the prospective trajectories were also identified from the

retrospective trajectories. The only PB1 signature mutation, PB1-R327K, separating swine viruses from human viruses was found from both the retrospective and prospective trajectories. Three PB2 signatures were also identified from both the retrospective and prospective trajectories. These findings suggest that the predicted evolutionary trajectories produced by prospective simulations are rather consistent with the retrospective evolutionary trajectories. Furthermore, it is noteworthy that there was a marked rise in the frequency of mutations on the signatures during 1990-2000 and 2001-2010, as shown in Tables 2 and 3, which was consistent with the time when the triple reassortment events occurred.

4 CONCLUSIONS

We proposed a grid-based simulation model to analyze and predict the evolutionary trends of IAVs. Unlike previous approaches based on phylogenetic trees or complex dynamics models, the proposed simulation model only involves a series of adaptive walks controlled by stochastic point mutations constrained within an evolutionary grid. The experiments of both interspecies transitions and genomic signature mutations have demonstrated promising results. It warrants further investigation into the applicability of the simulation model for predicting the evolutionary trends of IAVs.

ACKNOWLEDGEMENTS

The research was partially supported by Ministry of Science and Technology of Taiwan (MOST 108-2221-E-009-086).

REFERENCES

Brown, I. H., Harris, P. A., McCauley, J. W., Alexander, D.J., 1998. Multiple genetic reassortment of avian and human influenza A viruses in European pigs, resulting in the emergence of an H1N2 virus of novel genotype. J. Gen. Virol. 79, pp. 2947–2955.

Gerrish, P., 2001. The rhythm of microbial adaptation. Nature, vol. 413, pp. 299–302.

Gillespie, J. H., 1983. A simple stochastic gene substitution process. Theor. Popul. Biol. 23:202–215.

Gillespie, J. H., 1991. *The causes of molecular evolution*. Oxford Univ. Press, Oxford, U.K.

Hu, Y., Tu, P., Lin, C., Guo, S., 2014. Identification and Chronological Analysis of Genomic Signatures in Influenza A Viruses. Plos ONE, 9(1), e84638.

Lässig, M., Łuksza, M., 2014. Adaptive Revolution: Can we read the future from a tree. eLife Sci., 3, e05060.

Li, W., Godzik, A., 2006. Cd-hit: a fast program for clustering and comparing large sets of protein or nucleotide sequences. Bioinformatics, vol. 22(13), pp. 1658–1659.

Łuksza, M., Lässig, M., 2014. A Predictive Fitness Model for Influenza. Nature, 507, pp. 57–61.

Miotto, O., Heiny, A. T., Albrecht, R., Garcı´a-Sastre, A., Tan, T.W., et al., 2010. Complete-Proteome Mapping of Human Influenza A Adaptive Mutations: Implications for Human Transmissibility of Zoonotic Strains. PLoS ONE 5(2): e9025.

Naffakh, N., Tomoiu, A., Rameix-Welti, M-A, van der Werf, S., 2008. Host Restriction of Avian Influenza Viruses at the Level of the Ribonucleoproteins. Annu. Rev. Microbiol 62: 403-424.

Neverov, A. D., Kryazhimskiy, S., Plotkin, J. B., Bazykin, G. A., 2015. Coordinated Evolution of Influenza A Surface Proteins. PLoS Genetics, 11(8), e1005404.

Orr, H. A., 2002. The distribution of fitness effects among beneficial mutations. Genetics, vol. 163, pp. 1519–1526.

Orr, H. A., 2002. The population genetics of adaptation: the adaption of DNA sequences. Evolution, 56(7), pp. 1317–1330.

Orr, H. A., 2006. The population genetics of adaptation on correlated fitness landscapes: the block model. Evolution, 60(6), pp. 1113–1124.

Pan, C., Cheung, B., Tan, S., Li, C., Li, L., et al., 2010. Genomic Signature and Mutation Trend Analysis of Pandemic (H1N1) 2009 Influenza A Virus. PLoS ONE 5(3): e9549.

Perelson, A. S., Macken., C. A., 1995. Protein evolution on partially correlated landscapes. Proc. Natl. Acad. Sci. USA 92, pp. 9657–9661.

Smith, G. J. D. et al., 2009. Origins and evolutionary genomics of the 2009 swine-origin H1N1 influenza A epidemic. Nature, Vol. 459, pp. 1122–1126.

Timofeeva, T. A., Asatryan, M. N., Altstein, A. D., Narodisky, B. S., Gintsburg, A. L., Kaverin, N. V., 2017. Predicting the Evolutionary Variability of the Influenza A Virus. ACTA NATURAE, Vol. 9, No. 3(34), pp. 48–54.